Review

Multi-Global Navigation Satellite System for Earth Observation: Recent Developments and New Progress

Shuanggen Jin [1,2] **, Xuyang Meng** [1] **, Gino Dardanelli** [3,*] **and Yunlong Zhu** [1]

1   School of Surveying and Land Information Engineering, Henan Polytechnic University, Jiaozuo 454003, China; sgjin@shao.ac.cn (S.J.); 212204020068@home.hpu.edu.cn (X.M.); 212204020086@home.hpu.edu.cn (Y.Z.)
2   Shanghai Astronomical Observatory, Chinese Academy of Sciences, Shanghai 200030, China
3   Department of Engineering, University of Palermo, Viale delle Scienze, 90128 Palermo, Italy
*   Correspondence: gino.dardanelli@unipa.it

Abstract: The Global Navigation Satellite System (GNSS) has made important progress in Earth observation and applications. With the successful design of the BeiDou Navigation Satellite System (BDS), four global navigation satellite systems are available worldwide, together with Galileo, GLONASS, and GPS. These systems have been widely employed in positioning, navigation, and timing (PNT). Furthermore, GNSS refraction, reflection, and scattering signals can remotely sense the Earth's surface and atmosphere with powerful implications for environmental remote sensing. In this paper, the recent developments and new application progress of multi-GNSS in Earth observation are presented and reviewed, including the methods of BDS/GNSS for Earth observations, GNSS navigation and positioning performance (e.g., GNSS-PPP and GNSS-NRTK), GNSS ionospheric modelling and space weather monitoring, GNSS meteorology, and GNSS-reflectometry and its applications. For instance, the static Precise Point Positioning (PPP) precision of most MGEX stations was improved by 35.1%, 18.7%, and 8.7% in the east, north, and upward directions, respectively, with PPP ambiguity resolution (AR) based on factor graph optimization. A two-layer ionospheric model was constructed using IGS station data through three-dimensional ionospheric model constraints and TEC accuracy was increased by about 20–27% with the GIM model. Ten-minute water level change with centimeter-level accuracy was estimated with ground-based multiple GNSS-R data based on a weighted iterative least-squares method. Furthermore, a cyclone and its positions were detected by utilizing the GNSS-reflectometry from the space-borne Cyclone GNSS (CYGNSS) mission. Over the years, GNSS has become a dominant technology among Earth observation with powerful applications, not only for conventional positioning, navigation and timing techniques, but also for integrated remote sensing solutions, such as monitoring typhoons, river water level changes, geological geohazard warnings, low-altitude UAV navigation, etc., due to its high performance, low cost, all time and all weather.

Keywords: GNSS; geohazards; GNSS meteorology; GNSS ionosphere; GNSS-reflectometry

1. Introduction

After more than four decades of experimentation, as both GPS (Global Positioning System) beforehand and GNSS now, this technology represents an essential component based on several human efforts. In fact, whereas previously GPS only provided navigation, positioning and timing, nowadays GNSS satellite signals are used in new and innovative ways. One aspect comprises Earth Observation (EO) and remote sensing, defined as the gathering of environmental data regarding the physical, chemical, and biological systems of our planet. These sets of information are collected using sensors directly connected to the ground, airborne platforms (such as balloons and airplane), and satellites, with data often being derived from satellite imagery [1,2].

Alongside classic topics of scientific applications such as geodesy, geohazards, GNSS-NRTK (network real-time kinematic), and PPP (precise point positioning), it was thought

that major emerging applications such as those arising from, for example, GNSS-R Remote Sensing with SmallSats (BuFeng-1, CYGNSS, Fengyun-3C, FormoSat-7/COSMIC-2 (FS7/COSMIC2), FSSCat, HydroGNSS, PRETTY, and the Spire CubeSats series) might be of interest for the new applications, considering that remote sensing capabilities relative to the Earth are being tested and applied by these new satellites through the use of advanced payload technologies. The ECOSTRESS and SMAP satellites, for instance, were mainly designed to acquire information on soil moisture in areas covered by dense forests, representing a significant advancement in this developing field [3].

In this paper, the most recent results and the state of the multi-GNSS art for Earth observation are presented and reviewed, including but not limiting to, the following topics: tropospheric and ionospheric observations; modelling and assimilation from terrestrial and space-based GNSS observations; multi-GNSS NRTK, PPP, and PPP-RTK theories and methods; analysis of errors; systematic effects in the new GNSS solutions; and GNSS reflected signals and radio occultation, as well as the new applications for these technologies. Section 2 shows the technique and methods of BDS/GNSS for Earth observations, recent developments and new progress are presented in Section 3, and finally conclusions and future prospects are given in Section 4.

2. BDS/GNSS for Earth Observations

BDS/GNSS for Earth observation includes GNSS PPP, GNSS-RTK, GNSS-RO (radio occultation) with LEO satellites, GNSS ionosphere monitoring, GNSS meteorology, and GNSS-R (reflectometry), which are certainly the most current topics in the field of GNSS observations and scientific applications.

In BDS/GNSS Earth observation, GNSS technology is used to obtain the required information, for which GNSS raw observations are used. The GNSS observation equation describes the linear or non-linear relationship between the pseudo-range and phase observations and the unknown parameters, which is the basis of GNSS data processing. The observation equation can be expressed as

$$P^s_{r,j} = \rho^s_r + t^s_r + dt_r - dt^s + u_j I^s_r + d_{r,j} - d^s_j + \varepsilon^s_{p,j} \tag{1}$$

$$\varnothing^s_{r,j} = \rho^s_r + t^s_r + dt_r - dt^s - u_j I^s_r + \lambda_j N^s_{r,j} + \delta_{r,j} - \delta^s_j + \varepsilon^s_{\varnothing,j} \tag{2}$$

where r, s, and j represent the receiver, satellite, and frequency, respectively; $P^s_{r,j}$ represents the pseudo-range; $\varnothing^s_{r,j}$ represents the phase observation; $\rho^s_{r,j}$ represents the distance from the satellite to the receiver; $t^s_{r,j}$ represents the tropospheric delay from the satellite to the receiver; dt_r represents the receiver clock error; dt_s represents the satellite clock error; I^s_r is the ionospheric delay; λ_j is the wavelength of the phase at the j-th frequency carrier; u_j is the conversion factor of the ionosphere at j frequency; $d_{r,j}$ and d^s_j are receiver code deviation and satellite code deviation, respectively; $\delta_{r,j}$ and δ^s_j are receiver phase deviation and satellite phase deviation; $N^s_{r,j}$ is the phase ambiguity; and $\varepsilon^s_{p,j}$ and $\varepsilon^s_{\varnothing,j}$ are random noises.

2.1. GNSS Positioning

Primarily, GNSS positioning includes single point positioning (SPP), precise-point positioning (PPP), differential positioning (DGNSS), and real-time kinematic (RTK) positioning techniques. Single point positioning is based on a single GNSS receiver, using pseudorange observations and satellite broadcast ephemerides, without the requirement for an external reference station. It is suitable for mass-market positioning applications, with positioning accuracy typically ranging from several meters to tens of meters [4]. Differential GNSS (DGNSS) relies on a reference station to correct positioning errors at the user's location, improving the accuracy by reducing the errors caused by the atmospheric signal propagation. Real-time kinematic (RTK) positioning attains high accuracy by utilizing the differences in carrier phases between a mobile receiver and a reference station located on the ground. It requires real-time data transmission to

maintain centimeter-level accuracy [5]. Conversely, precise point positioning (PPP) relies on an exact satellite orbit and clock corrections, without needing ground GNSS network stations. Nonetheless, it needs accurate data in order to correct satellite-orbit and clock errors. PPP is ideal for rapid deployment, with accuracy reaching the centimeter level [6].

The implementation of PPP in global or regional scale is significantly supported by the presence of continuous networks of reference stations, known as CORS (Continuously Operating Reference Station), which provide free data for scientific purposes. A recent study conducted by Radicioni et al. demonstrated the abilities of various next-generation, low-cost, multi-constellation, and multi-frequency GNSS sensors, utilizing only the permanent GNSS-CORS multi-constellation stations located in Umbria, Italy [7]. Baybura et al. conducted several experiments comparing PPP-RTK, network RTK (NRTK), and long baseline-based RTK (LBRTK). The results showed that both the LBRTK and NRTK techniques delivered comparable performance for baselines up to 40 km, exhibiting discrepancies of under 3 cm horizontally and 4 cm vertically [8]. Lu et al. proposed a novel time-relative positioning algorithm, acknowledging that, as widely recognized, and the PPP technique offered high-precision positioning data but needed an initialization period of 10–30 min. In their approach, current epoch parameters such as the position vector and the ambiguities of the float ionosphere-free (IF) model were estimated. Results from numerical tests conducted during both static and dynamic conditions revealed that the proposed positioning algorithm achieved an accuracy of just a few centimeters within one hour. It is evident that by combining GPS, BeiDou, and Galileo, the positioning accuracy was significantly improved, due to the increased number of satellites and a more favorable geometric distribution concerning DOP (Dilution of Precision) [9]. In contrast, Zhang and Odijk introduced a novel approach for network processing, which achieved single-frequency PPP-RTK. Tests conducted with daily GNSS data gathered from a CORS network, along with a single-frequency rover receiver (u-blox), demonstrated that the success rate for ambiguity resolution in the CORS network reached 98.89% [10].

Recently, an intriguing review has been published on selected topics related to GNSS CORS, including structure monitoring, accuracy, network monitoring, and reference frames. Given the extensive range of articles discussed in this work, readers are encouraged to pursue further research on the subject [11]. An intriguing study was presented by Angrisano et al. [12], which demonstrated the efficacy of the multi-GNSS PPP method in a static configuration. This research utilized the free, open-source software RTKLib (version 2.4.2 p13), including satellite orbits and accurate clock data from CLS (Collecte Localisation Satellitique) and CNES (Centre National d'Etudes Spatiales). Additionally, two distinct tropospheric models were evaluated: the estimated ZTD (Zenith Tropospheric Delay) model and the traditional Saastamoinen model. The findings indicated a significant improvement in the performance of GNSS combinations (including single systems such as Galileo-only, GLONASS-only, and GPS-only, as well as dual combinations like GLONASS + GPS, Galileo + GPS, Galileo + GLONASS, and the triple combination of Galileo + GLONASS + GPS) relative to single-GNSS scenarios [12].

Some comparisons between NRTK, PPP, and static surveys (using the latter as a reference), using some benchmark points, were presented in [13]. NRTK positioning was achieved by different methods (VRS and FKP), while PPP solutions were computed with two types of software (CSRS, version 3 and RTKLib). A thorough statistical analysis was conducted to determine whether the frequency distribution of the residuals of the coordinates aligned with a normal distribution across all tested pairs. The findings indicated that the normal distribution hypothesis was supported in the majority of comparisons. Specifically, the Static-versus-NRTK pairs exhibited the highest level of consistency, while the pairs generated with the CSRS software demonstrated better consistency when compared to those derived from the RTKLIB software, based on the PPP solutions [13–15].

GNSS PPP is commonly utilized because of its affordability and the possibility of quick implementation. Currently, the observation models commonly used in PPP can

generally be separated into two main sections: combined and non-combined models. Combined models include the ionosphere-free combination model and the UofC model, while non-combined models are based on original GNSS observations. The conventional ionosphere-free (IF) synthesis of dual-frequency measurements effectively eliminates the first-order ionospheric delay, thereby greatly minimizing the effect of ionospheric delay on GNSS measurements. As a result, this synthesis is widely utilized in PPP for positioning solutions. The observation equation can be articulated as follows [16,17].

$$P^s_{r,j} = \frac{f_1{}^2}{f_1{}^2 - f_2{}^2} P_1 - \frac{f_2{}^2}{f_1{}^2 - f_2{}^2} P_2 = \rho^s_{r,j} + c(dt_r - dt_s) + t^s_{r,j} + \varepsilon^s_{p,j} \tag{3}$$

$$\varnothing^s_{r,j} = \frac{f_1{}^2}{f_1{}^2 - f_2{}^2} \varnothing_1 - \frac{f_2{}^2}{f_1{}^2 - f_2{}^2} \varnothing_2 = \rho + c(dt_r - dt_s) + t^s_{r,j} + \lambda_j \cdot N^s_{r,j} + \varepsilon^s_{\varnothing,j} \tag{4}$$

where $P^s_{r,j}$ is the pseudorange measurement, $\varnothing^s_{r,j}$ refers to the carrier-phase measurement, c is the speed of light in a vacuum, $\rho^s_{r,j}$ represents the distance between the receiver and the satellite, $t^s_{r,j}$ refers to tropospheric delay, dt_r is the receiver clock error, dt_s is the satellite clock error, λ_j is the carrier wavelength, and $N^s_{r,j}$ is the integer ambiguity. The frequencies associated with the L1 and L2 carrier-phase measurements are f_1 and f_2. Finally, $\varepsilon^s_{p,j}$ and $\varepsilon^s_{\varnothing,j}$ represent the noise in both the pseudorange and carrier-phase observations.

In recent years, with the processing of GNSS, both the ionosphere-free model and the UofC model have been expanded to handle multi-frequency signals with achieving excellent results. The UofC model is another type of observation that eliminates ionospheric effects through a combination-based method, as proposed by the University of Calgary, Canada [18]. The model leverages an important characteristic of the ionospheric delay's impact on satellite observations. Specifically, it recognizes that the ionospheric delay produces effects of equal magnitude but opposite sign on two types of measurements: pseudorange and phase observations. By implementing a process within which each pseudorange measurement is averaged with its corresponding phase observation at the same frequency, the model effectively removes the ionospheric delay in the pseudorange data. This technique enables the creation of two new combined pseudorange observations that are free from the influence of the ionosphere, providing more accurate and reliable data for further analysis.

The undifferenced and uncombined model uses the original observations to avoid the amplification of the observation noise caused by the data combination and the waste of some observation information. The mathematical model can make full use of the observation data information, and the observation noise is small. It can estimate both tropospheric and ionospheric delay, which is relevant for atmospheric monitoring. The undifferenced and uncombined model considers the short-term stability of the ionosphere, and the ionospheric parameters between epochs can be used as weak constraints to improve the robustness of the observation equation. In the case of accurately known ionospheric delay information, the ionospheric delay can be used as a known quantity to constrain the observation equation and improve the convergence time of the precise-point positioning.

2.2. GNSS Radio Occultation

GNSS radio occultation refers to a remote sensing method to acquire atmospheric information. This process involves the use of a GNSS receiver installed on a Low Earth Orbit (LEO) satellite, which captures electromagnetic wave signals emitted by a high-orbit GNSS satellite, with the objective of probing the elements of the Earth's atmosphere. The LEO satellite orbits the Earth and consistently collects GNSS signals. As the GNSS signal travels toward the LEO satellite, it traverses the Earth's ionosphere and neutral atmosphere, resulting in a change in the signal's path due to refraction, which causes a phase delay.

This technology does not rely on ground stations and can provide atmospheric profile data on a global scale with high levels of precision. GNSS radio occultation detection is not sensitive to weather conditions and can be observed under various climatic conditions. This technique is widely used in meteorology, climate research, and space weather monitoring. For instance, researchers can examine how solar activity impacts the Earth's electromagnetic environment by investigating variations in the ionosphere. Additionally, by utilizing refraction data from the neutral atmosphere, one can observe fluctuations in meteorological factors like temperature and humidity.

GNSS radio occultation has been widely used in monitoring tropospheric and ionospheric changes. Li et al. [19] successfully developed a highly precise empirical three-dimensional Global Electron Density Model (GEDM) by utilizing the COSMIC GNSS radio occultation dataset, employing advanced techniques such as Fourier expansion and principal component analysis (PCA) for their analysis. Their work involved a rigorous evaluation of the GEDM model against the well-established IRI-2020 model. The results of the evaluation indicated that the GEDM model exhibited a significantly higher degree of consistency when compared to the IRI-2020 model. The statistical error associated with the GEDM model is markedly lower than that of the IRI-2020, particularly in mid-latitude regions where ionospheric conditions often vary. Furthermore, the GEDM model demonstrated an exceptional capability to accurately represent key ionospheric features, including the Equatorial Ionization Anomaly (EIA), the seasonal winter anomaly, and the annual anomaly. These findings underscore the GEDM model's potential as a superior tool for ionospheric research and applications. The role of GNSS radio occultation is significant in meteorological forecasting. Wang and Jin [20] examined how GNSS radio occultation observations influenced the prediction of the severe rainstorm that struck Henan, China, on 20 July 2021. Their findings suggest that the incorporation of GNSS radio occultation data can enhance the accuracy of precipitation distribution and amount forecasts, thereby improving the predictions for events such as this unprecedented rainfall event.

2.3. GNSS Ionosphere Monitoring

GNSS ionospheric monitoring is a technology that uses GNSS signals to observe and analyze the states and variations of the ionosphere. For a long time, scientists have been monitoring the ionosphere mainly through ionospheric altimetry, radar, sounding rockets, and other detection instruments, but these traditional methods have some limits. GNSS has the characteristics of all-weather functionality, high efficiency, and low cost. It is capable of tracking whole ionospheric activity over an extended time series, offering a crucial foundation for uncovering the temporal and spatial distribution of ionospheric Total Electron Content (TEC) variations and understanding the patterns of ionospheric activity.

Given the different operating positions of GNSS signal-receiving equipment, ionospheric monitoring technology may be divided into ground-based and space-based GNSS detection. Ground-based GNSS detection is based upon a signal receiver on the ground. Nowadays, there are more GNSS tracking stations on the ground. The largest and most extensively distributed network of ground-based stations is represented by the International GNSS Service (IGS). Currently, there are more than 500 IGS stations worldwide. Additionally, due to the swift advancement of GNSS technology, the IGS has started the establishment of a multi-GNSS observation network that operates across multiple frequencies and systems (MGEX). In addition to the global GNSS network, different countries and regions have also established their own regional GNSS networks. The EUREF Permanent GNSS Network, the Crustal Movement Observation Network of China, and the Australian Regional GNSS Network are notable examples of existing ground-based GNSS systems. These networks utilize global ground-based GNSS technology to monitor the ionosphere, offering robust all-weather observation data. However, a significant limitation of these ground-based GNSS stations is their predominant distribution over land areas, which results in a notable scarcity of observation data collected

over oceanic regions. To overcome this limit, space-based GNSS ionospheric monitoring technology has been developed, which is able to provide comprehensive measurements over oceans, where ground-based data is lacking. The space-based GNSS observation is a new technology that utilizes a signal receiver on a LEO satellite to monitor the ionosphere and thereby realizes the remote sensing of the ionosphere. According to the mutual motion of the satellites and the Earth, when the radio occultation occurs, the GNSS receiver can obtain information such as TEC and bending angle at different heights, and then invert the ionospheric electron density parameters. A series of geo-orbiting satellites with GNSS occultation observation capabilities have been launched internationally, such as CHAMP, COSMIC, GRACE, Fengyun-3C and Metop-A/B/C. The connected facilities of space-based GNSS and ground-based GNSS have been widely used for ionospheric monitoring and research [21,22]. In the future, the establishment and development of more Earth-orbit satellites will also lay a foundation for ionospheric detection with high spatial and temporal resolution.

2.4. GNSS Meteorology

Tropospheric delay is one of the main error sources in GNSS positioning [23]. By utilizing ground-based GNSS stations alongside the BeiDou Navigation Satellite System, the technology of precise-point positioning (PPP) can effectively estimate tropospheric delay. In comparison to radiosonde data and the fifth-generation generation reanalysis data from the European Center for Medium-Range Weather Forecasts (ECMWF) (ERA5), the GNSS provides high precision and enables real-time descriptions of short-term fluctuations in regional tropospheric delay [24]. A critical parameter in climate research, Precipitable Water Vapor (PWV) serves as a commonly used standard measure of atmospheric water vapor content [25]. ZTD (Zenith Tropospheric Delay) is closely related to meteorological monitoring and early warning systems. By utilizing suitable methods, the tropospheric delay can be translated into PWV [26], which enables the assessment of atmospheric water vapor levels and provides dependable technical assistance for meteorological measurements. Studies have shown that the PWV in China exhibits clear seasonal variations (Figure 1), and this cyclical pattern provides a theoretical basis for PWV research. Therefore, the monitoring of PWV is essential for climate studies and for the ability to issue early warnings related to extreme weather events [27].

In GNSS meteorology applications, various meteorological parameters play crucial roles in the revealing of weather changes. These parameters include atmospheric pressure, vapor vapor, temperature, and weighted average temperature. The atmospheric weighted average temperature (Tm) is a critical parameter for the determination of PWV. Zhao et al. [28] developed a Tm model (LSTM-ERATM) utilizing a long short-term memory (LSTM) approach that leveraged atmospheric reanalysis data provided by the EAR5. The findings of their study indicated that this model delivered highly accurate temperature information tailored for users within the specified region. In comparison to existing models such as UNB3, GPT3, and Bevis, the LSTM-ERATM demonstrated a significant reduction in the root mean square error (RMS) during its validation against ERA5 data with achieving reductions of 50.8%, 37.4%, 26.2%, and 18.9%, respectively. Furthermore, when validated with radiosonde data, the LSTM-ERATM model also showed impressive performance, with RMS reductions of 31.3%, 27.2%, 35.9%, and 8.6% for the corresponding models. These results highlighted the superior accuracy of the LSTM-ERATM model in providing reliable temperature data.
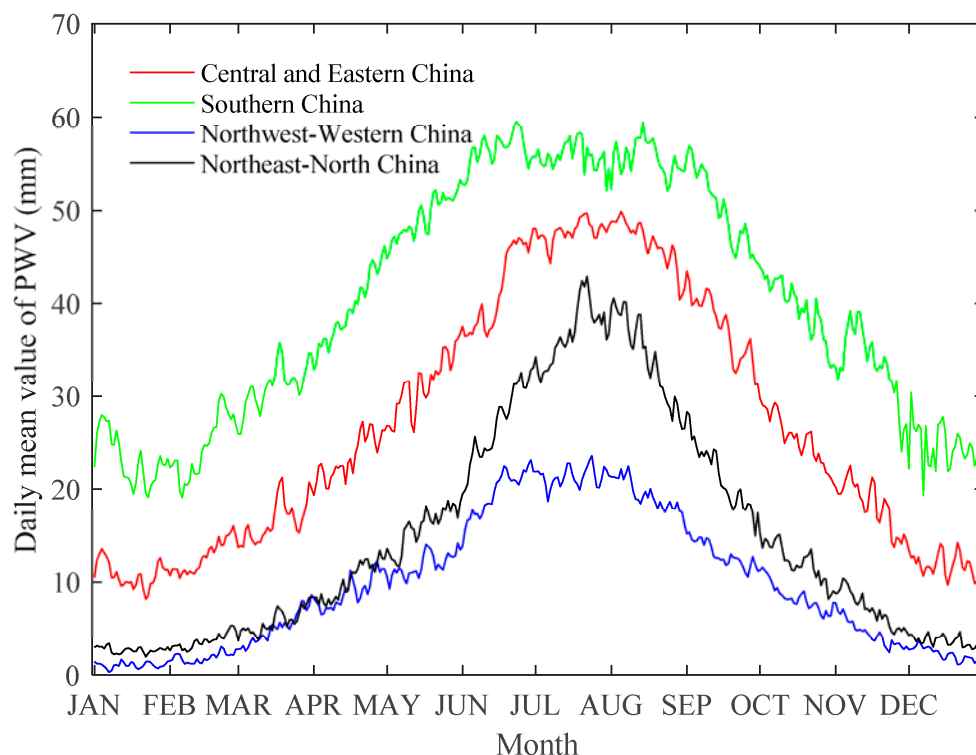
Figure 1. PWV variation trend in different regions of China from GNSS observations (Reprinted from Ref. [26]).

2.5. GNSS-Reflectometry

GNSS reflectometry (GNSS-R) is a technique that utilizes the reflective properties of GNSS signals for monitoring environmental conditions on the Earth's surface. This method can examine the variations between the signal transmitted directly from the satellite and the reflected signal from the surface and infer information as to the characteristics of the surface. The application of GNSS-R technology is widespread in the fields of environmental remote sensing, including hydrology, ice and snow, ocean environment, and vegetation coverage. GNSS-R technology is a remote sensing technology based on the principle of GNSS signal reflection. It uses the reflected GNSS signals from the surface of the ground or other objects and obtains information such as ground features and environmental parameters. Its principle is based on the reflection-based characteristics of GNSS signals upon reflection from the surface. For example, the characteristics of the reflected signals—such as delay, amplitude, phase, and frequency—vary according to the physical properties of the surface (like soil moisture, wave height, and ice thickness). By analyzing these variations, relevant information about the surface environment can be obtained. The benefits of GNSS-R include extensive coverage, functionality in all weather conditions, reduced expenses, and the capability to utilize current GNSS satellite signals for environmental observation through developing a vital instrument among remote sensing applications. GNSS-R can be classified into three distinct categories: ground-based GNSS-R, airborne GNSS-R, and space-borne GNSS-R. This classification is grounded in the varying methods and platforms of signal reception and the specific application contexts in which these systems operate. To illustrate this concept more concretely, we can consider ground-based GNSS-R, particularly its application for measuring sea surface height and water level change. The fundamental operating principle underlying this technique is depicted in Figure 2, which provides a visual representation of how ground-based GNSS-R is effectively working in this capacity.
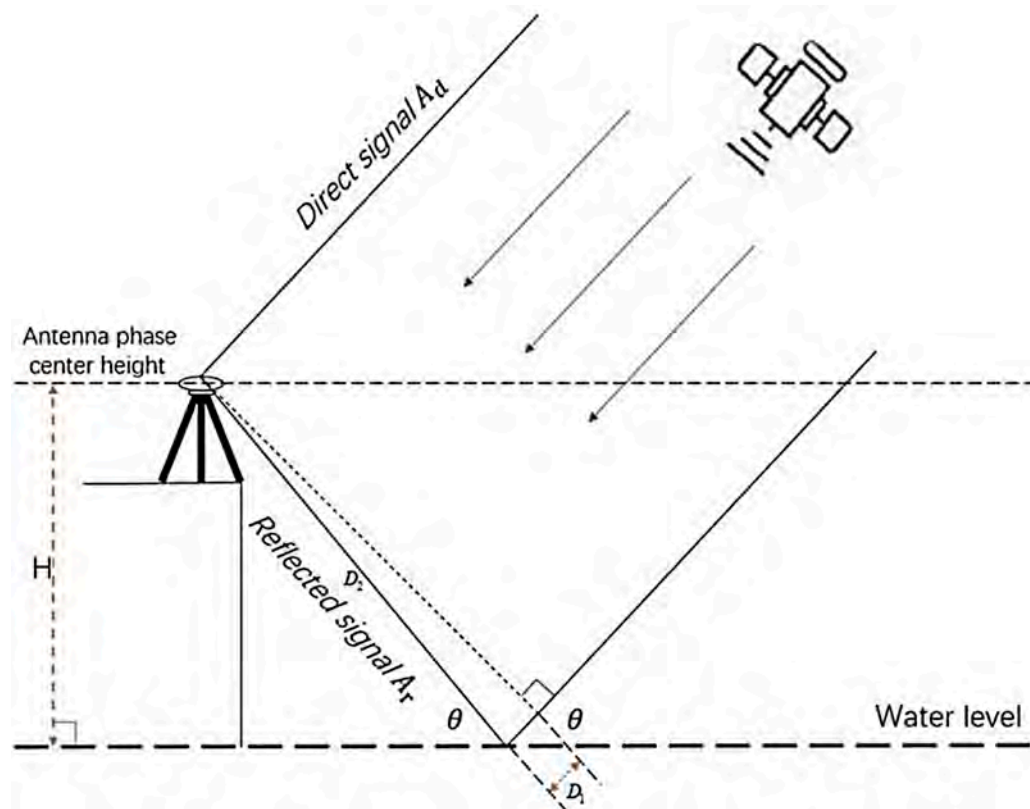
Figure 2. Geometric model of GNSS multipath reflectometry (GNSS-R).

3. Recent Developments and Progress

3.1. GNSS Positioning Performances

Multi-GNSS has been widely applied in navigation and positioning, as well as in tropospheric Zenith Tropospheric Delay (ZTD) estimation, e.g., using the low-cost Centipede-RTK network [29]. To ensure that the results were not influenced by any specific software, the researchers compared the ZTD calculations using two different open-source scientific software programs: RTKLIB (specifically, demo version 5) and CSRS-PPP (version 3). The findings from this evaluation were quite informative with revealing that the ZTD estimates derived from the Centipede-RTK network and the EPN were closely aligned when processed through the CSRS-PPP software. The maximum mean difference observed between the estimates from these two networks was approximately 3.5 cm. This close agreement highlighted the reliability and the coherence of the ZTD calculations obtained from both systems, thereby suggesting the effectiveness of the methodologies employed in the research [29].

Furthermore, the GNSS positioning capabilities were enhanced through case studies of GNSS RTK with the selection of basis functions for the adjustment of unmodelled errors and a required step aiming to deliver a conceptual basis and technical recommendations for the subsequent implementation of specific time-varying models. To achieve this goal, three fundamental functions—sinusoidal, polynomial, and combinatorial—were examined to fit unmodeled errors in differential placements. The datasets were obtained and tested by the IGS and the NOAA's IFCORS (US National Oceanic and Atmospheric Administration) [30].

A different study examined the precision of the tilt compensation feature in GNSS/IMU receivers within an open-air setting. Gučević et al. [31] sought to inform professionals and researchers about the specifications and limitations associated with employing GNSS/IMU technology for precise measurements, so as to avoid compromising the accuracy of coordinates in GNSS RTK surveys. The experiment utilized seven GNSS/IMU receivers, which had compensation angles α ranging from 30° to 45°.

The precision positioning status of low-cost GNSS receivers and geodetic GNSS receivers under different working conditions were evaluated, using fast and real-time satellite products for experiments, respectively [32]. In motion mode, the combined GNSS PPP utilizing GPS and GLONASS, along with the 'WHU' fast product, achieved centimeter-level positioning accuracy across various directions. An analysis of convergence times indicates that the PPP based on either GPS or BDS, when employing 'WHU' products alongside geodetic receivers, requires approximately 38.2 min. In contrast, when employing a dual system, this time is reduced to approximately 18.5 min, and with a triple system, it can be further reduced to 14.8 min. When utilizing static data, the influence of multi-GNSS combinations on convergence time is limited, and mainly depends on the accuracy of the products employed. For motion-based PPP that utilizes low-cost GNSS receivers, achieving an extreme precision of below 0.1 m typically necessitates over two hours, which is considerably longer than the convergence times observed at the MGEX site. It is noted that the convergence time for multi-GNSS PPP is shorter when compared to single-system PPP (see Figure 3), and the convergence time for fixed solutions is superior to that of floating-point solutions (see Figure 4).
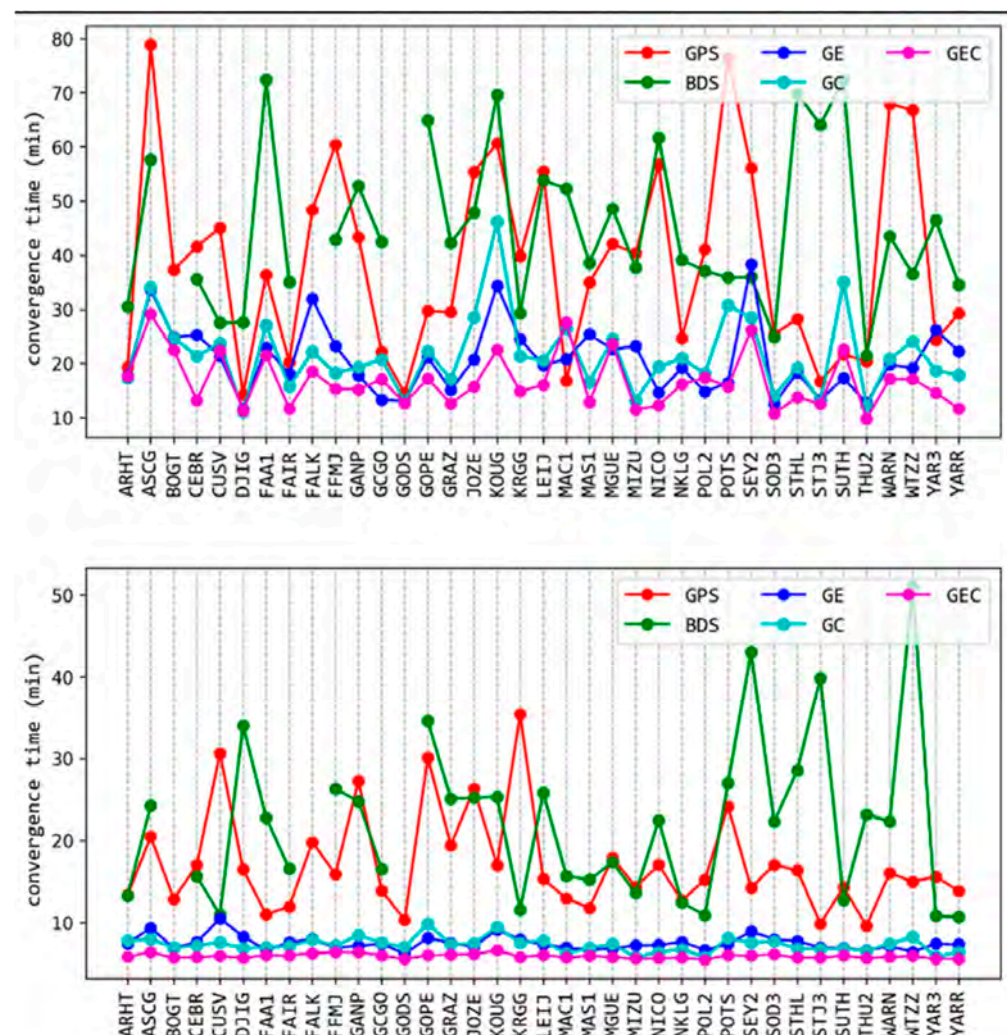

Figure 3. Convergence time using different system combinations and 'GBM' products with the average floating-point solution (**top**) and fixed solution (**bottom**) at each site (Reprinted from Ref. [32]).
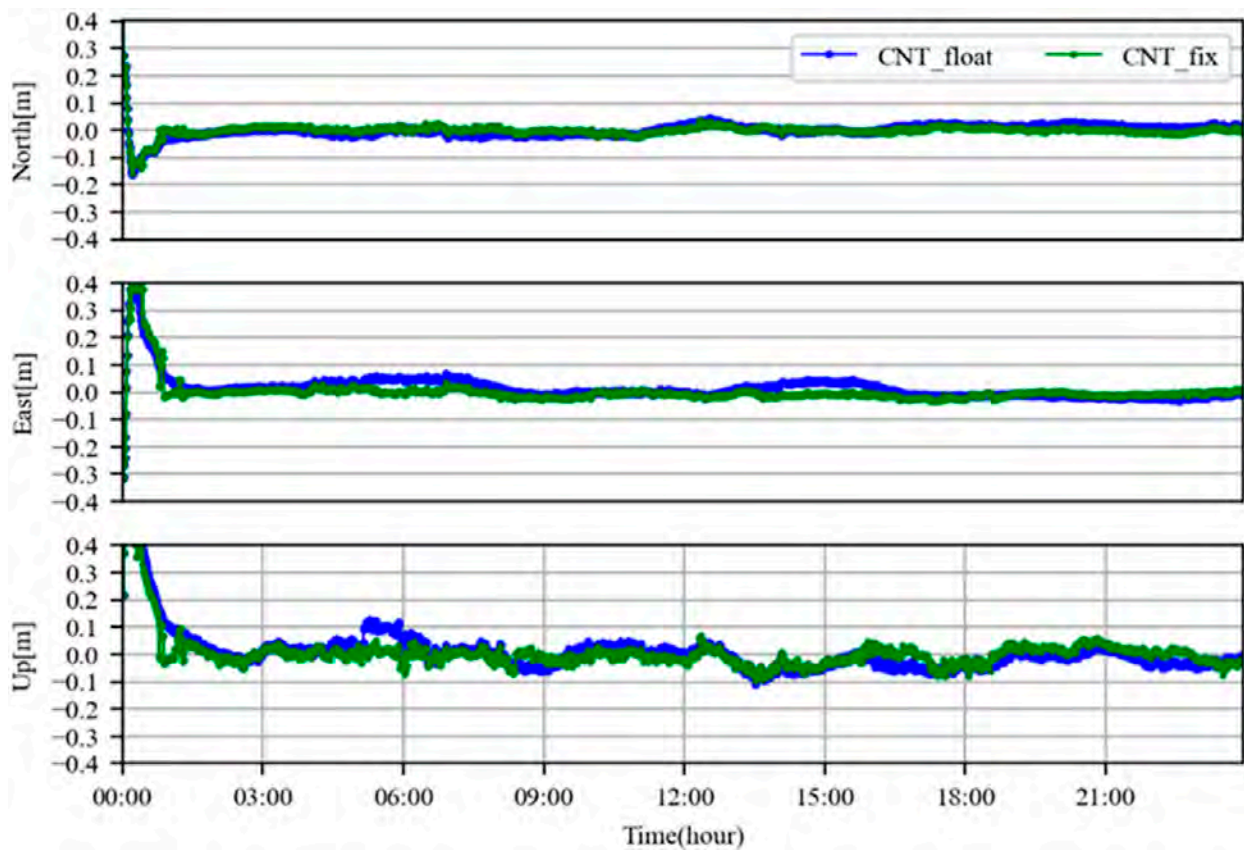
Figure 4. The positioning-error sequence of dynamic PPP by using the ambiguity floating point solution and the ambiguity-fixed solution of real-time products (Reprinted from Ref. [32]).

Cui et al. [33] established a high-precision tropospheric delay model using ground-based GNSS stations and the MOFC model, and applied it to PPP, which improved the positioning accuracy and convergence time of PPP-AR (Figure 5). The MOFC model with different reference-station densities was further evaluated in GPS and Galileo kinematic PPP-AR solutions. Compared with the PPP-AR solution without tropospheric delay enhancement, the positioning accuracy levels of the MOFC and OFC schemes with a 100 km inter-station distance were improved by 25.7% and 17.8%, respectively, while the corresponding times-to-first-fix (TTFFs) in high-altitude areas were improved by 36.9% and 33.0%.
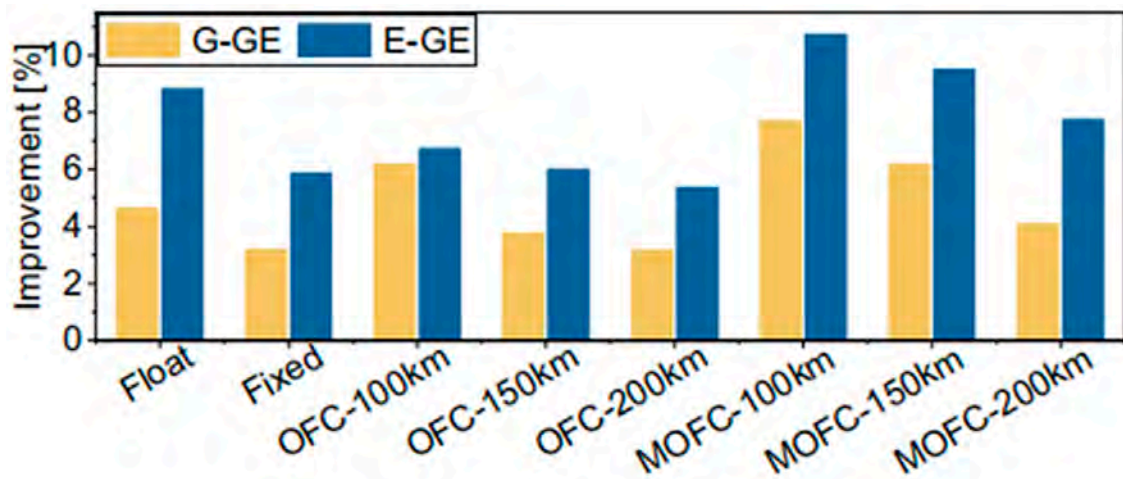

Figure 5. The positioning accuracy of the GPS + Galileo combined solution is improved in kinematic PPP when compared to the GPS-only and Galileo-only solutions (Reprinted from Ref. [33]).

Xiao et al. [34] proposed a PPP-AR based on factor graph optimization, in which the pseudorange and carrier-phase factors are constructed from the error equations of the raw observations, while the ambiguity resolution factor is constructed from the ambiguity resolution process. Validation results from most MGEX stations showed that the average precision of static PPP was improved from 1.25 cm, 0.61 cm, and 2.29 cm to 0.81 cm, 0.5 cm, and 2.1 cm, corresponding to improvements of 35.1%, 18.7%, and 8.7% in the eastward, northward, and upward directions, respectively (Figure 6).
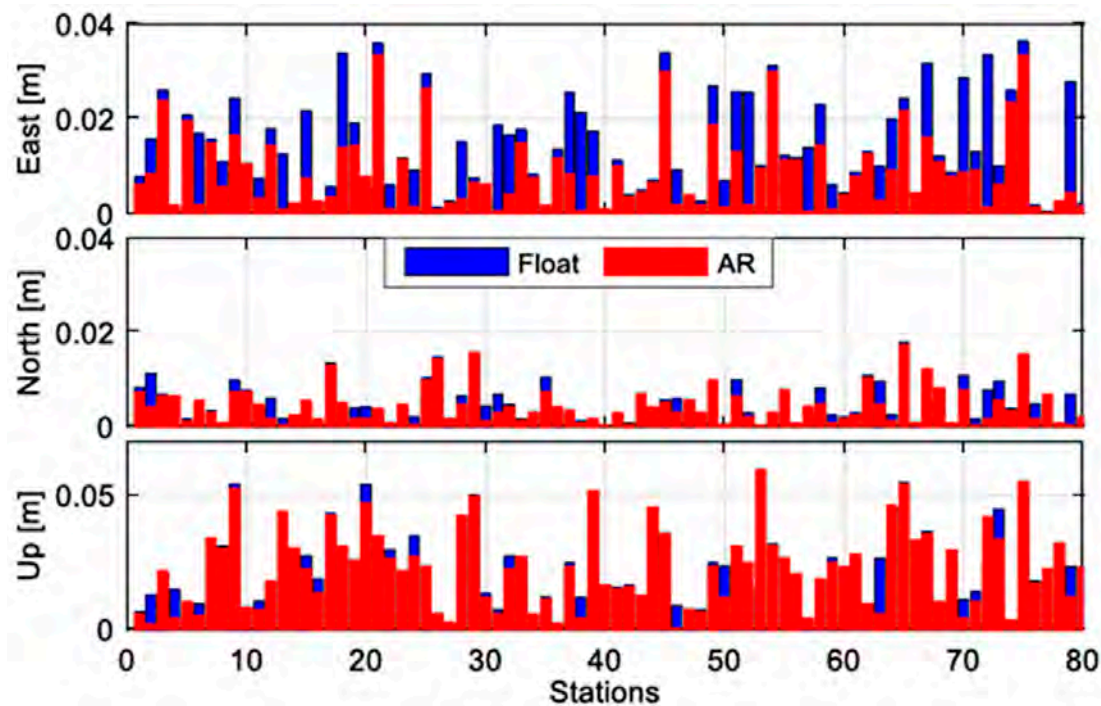

Figure 6. Static positional biases of AR and float solutions for MGEX stations on DoY 183, 2022 (Reprinted from Ref. [34]).

3.2. Atmospheric Sounding by GNSS-RO

GNSS-RO is a satellite remote sensing method utilizing GNSS radio occultation observations from various signals such as GPS, GLONASS, Galileo, and BDS. These signals are gathered from low-orbit satellites to estimate the Earth's atmospheric parameters (including the ionosphere and troposphere) with a high degree of vertical precision. The high vertical resolution of GNSS-RO data provides a good opportunity to study space weather and ionospheric variations, and atmospheric characteristics, or climate monitoring and model validation. A case study has been conducted utilizing a virtual testing platform to enhance the sustainable product development of GNSS-RO signal receivers. The purpose was the implementation of GNSS radio occultation observations, using the innovative satellite FengYun-3C, or FY-3C, one of the world's most important civilian meteorological satellites, which was utilized for both morning and evening orbits. The outcome was more compelling when compared to results at the altitude spectrum of 0–5 km. Findings ensured that the relative error remained below 2%, whereas in the subsequent altitude range of 5–20 km, the relative error dropped to under 1% [35].

Also, commercial GNSS-RO satellites (the American PlanetiQ, the Korean KOMPSAT-5, and the Spanish PAZ) were evaluated in terms of coverage, SNR, and penetration depth. The results showed that the capability of PlanetiQ was approximately equal to those of KOMPSAT-5 and PAZ, especially with respect to the tracking of signals from any GNSS satellite. Additionally, PlanetiQ performed more strongly in the deepest troposphere [36].

3.3. GNSS Ionospheric Sounding

The global ionospheric map was derived from the global international GNSS service (IGS) observation data. Wang et al. [37] compared the precision of global ionospheric maps produced by different IGS analysis centers with observational datasets from the MGEX and the IGS. The institutions and sources of data involved in this examination included the Chinese Academy of Sciences (CAS), the European Space Agency (ESA), the multi-mode and multi-frequency GNSS observations (MMG), the Jet Propulsion Laboratory (JPL), the Polytechnic University of Catalonia (UPC), and Wuhan University (WHU), while the ionospheric maps from the Center for Orbit Determination in Europe (CODE) serve as the benchmark standard [38]. Furthermore, the variability of the TEC was examined based on the discrepancies observed between the maps produced by the Ionospheric Associated Analysis Centers (IAACs) of the IGS and the altimetry-derived TEC obtained from an extensive dataset covering the period from 2005 to 2021 [39].

The equatorial plasma bubble (EPB) was observed in the temporal range of 2019–2023 based on the FS7/COSMIC-2 dataset, as to both equatorial and near low-latitude regions when considering a proposed hypothesis on seasonal versus longitudinal variability [40]. Aa et al. [41] found that the occurrence rate of EPBs was increased with increasing geomagnetic activity based on the data statistics from the Swarm satellite from 2013 to 2019. Zhao et al. [42] analyzed the dependence of equatorial plasma bubbles on solar and geomagnetic activities and seasons by using the long-term global observation data of GNSS TEC monitors in low latitudes. The results showed that the incidence of equatorial plasma bubbles in each longitude-based region of the world was significantly positively correlated with solar activity.

High-precision ionospheric monitoring and modeling is of great significance for satellite communication, satellite navigation, space weather monitoring, and so on. Nowadays, using GNSS signals to invert the ionospheric TEC is an important technical means for space weather monitoring [39], such as constructing a 2-D or 3-D global ionospheric model through GNSS technology. The precision of the worldwide ionospheric model is primarily affected by two factors: firstly, the source of observational data, which encompasses the quantity of puncture points, their spatial distribution, and the quality of the observational data; secondly, the modeling approach, which includes methods for data extraction, estimation techniques, algorithm reliability, and other related elements. The carrier-phase smoothing pseudorange method is a simple STEC extraction method [43]. With the frequency expansion of multi-GNSS, this method has also been applied to multi-frequency observations. In order to capture higher-precision ionospheric information, the use of PPP technology to extract STEC has been confirmed. In ionospheric modeling, the ionospheric TEC is typically expected to be on a thin layer at a fixed height, but this affects the accuracy of the model. Jiang et al. [44] established a two-layer ionospheric model (Figure 7) using IGS station data through three-dimensional ionospheric model constraints, and compared the results with the global ionospheric map (GIM). It was found that the TEC of the model was increased by about 20–27% with respect to the GIM model. Li et al. [45] constructed a three-dimensional electron density model (Figure 8) using COSMIC GNSS occultation data and showed a good performance by using a variety of independent data validation.

With the increase of multi-GNSS observational data, real-time ionospheric simulation has become more and more popular. Han et al. [46] carried out real-time ionospheric modeling based upon ground-based and space-borne data sources. In addition, there have also been some interesting advances in space-based monitoring of disaster-related weather by analyzing the characteristics of ionospheric TEC disturbances. Ma and Jin [47] conducted a detailed study and revealed the varying characteristics of ionospheric disturbances during Typhoon Chandu, utilizing data from GPS and GLONASS, including the amplitude of the disturbances and the speeds (Figure 9).
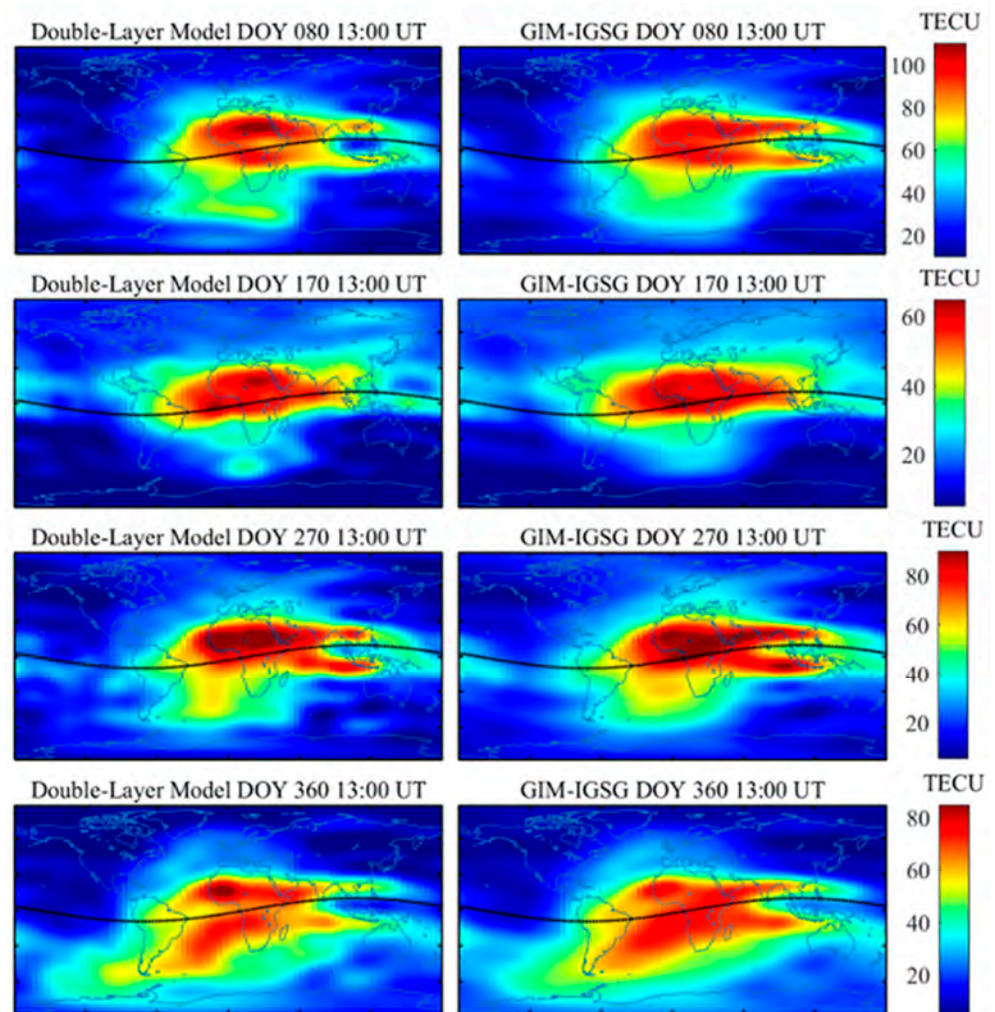
Figure 7. The spatial distribution of TEC at 13:00 UT during DOY 80, 170, 270, and 360 in 2023 for the double-layer SH model (**left**) and GIM-IGS (**right**) (Reprinted with permission from Ref. [44]. 2024 Jin, S.).
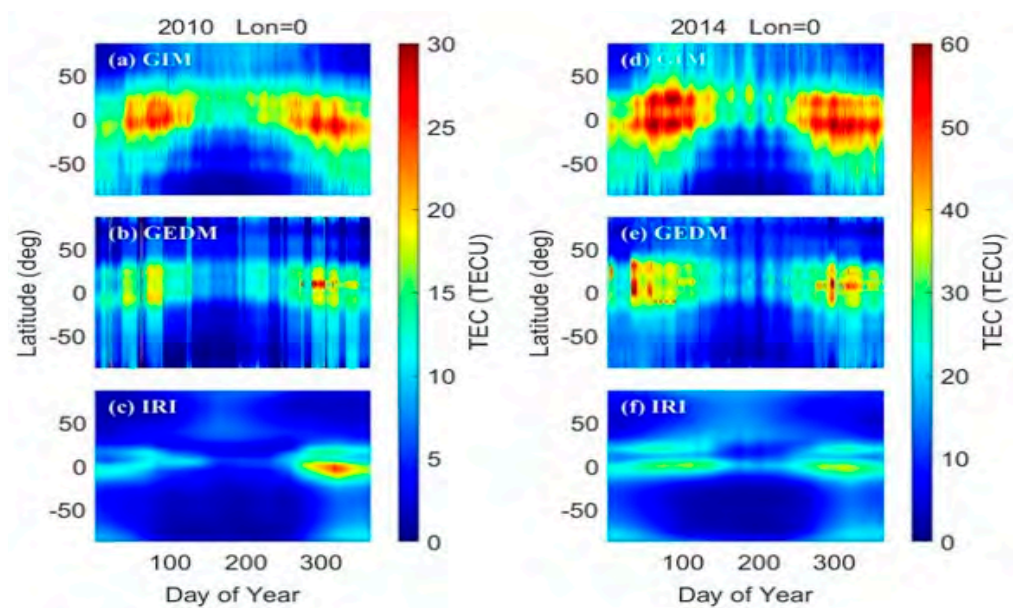

Figure 8. Daily average TEC from GIM, GEDM, IRI-2020 in 2010 (**left**), and 2014 (**right**) (Reprinted with permission from Ref. [45]. 2024 Jin, S.).
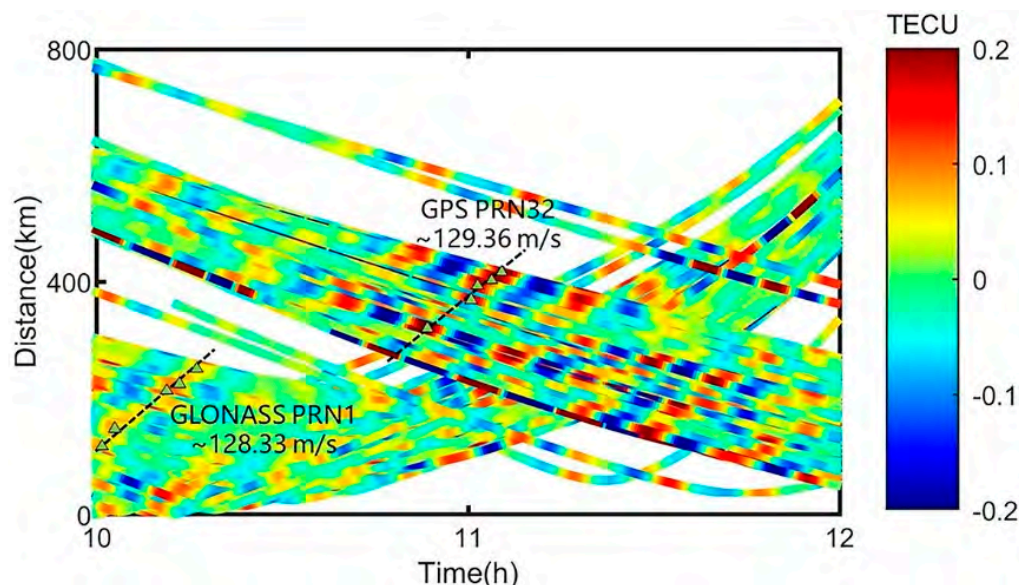
Figure 9. Ionospheric disturbance characteristics during Typhoon Chandu, from GPS PRN32 and GLONASS PRN1 (Reprinted with permission from Ref. [47]. 2024 Jin, S.).

3.4. Tropospheric Sounding by Ground-Based GNSS

The GNSS has established itself as a leading method for the detection of ZTD. The advent of new multi-GNSS frequencies, coupled with advancements in precise-point positioning ambiguity resolution (PPP-AR) technology, presents both significant opportunities and challenges in the high-precision retrieval of GNSS-ZTD. These developments are crucial, as they enhance the accuracy and reliability of ZTD measurements, thereby facilitating improved atmospheric modeling and numerous applications in meteorology and climatology. However, the complexity involved in the integration of multiple GNSS frequencies and optimizing the PPP-AR processes also requires ongoing research and innovation to fully harness the potential of these technologies.

Tropospheric delay usually refers to the signal delay generated by the electromagnetic wave signal when passing through the ionized neutral atmosphere below the height of 50 km. The delay is influenced by temperature, pressure, and humidity, as well as the locations of the receiver and transmitter antennas. The ZTD has been estimated based on the GNSS PPP method using MGEX stations over a period exceeding one year (Figure 10), which was assessed by using standard IGS tropospheric products, alongside radiosonde data and the ERA5 reanalysis dataset [24]. The ZTD time series derived from GPS were more consistent and precise when compared to those generated exclusively from the Galileo, BDS, and GLONASS solutions.

One study investigated the link between ZTD detected by ground-based GNSS and the La Nina phenomenon [48]. Firstly, the GNSS-ZTD retrieval features of all existing dual-frequency combinations was thoroughly examined. Then, taking the popular dual-frequency combination as an example, the influences of PPP-AR and system combination were analyzed. The results were not merely a reference for GNSS-ZTD retrieval, but also provided an in-depth understanding of the relationship between the occurrence of the La Nina phenomenon and the performance of GNSS-ZTD retrieval. The difference in the ZTD inversion between the checked IGS stations during the La Nina and non-La Nina times wa s computed and globally interpreted. The greater the RMSE difference was, the more dramatic the ZTD change was during La Nina. Compared with the non-La Nina period, the ZTD in the Pacific remained significantly stable, while the ZTD values in Antarctica, East Asia, North America and Oceania changed more dramatically (Figure 11).
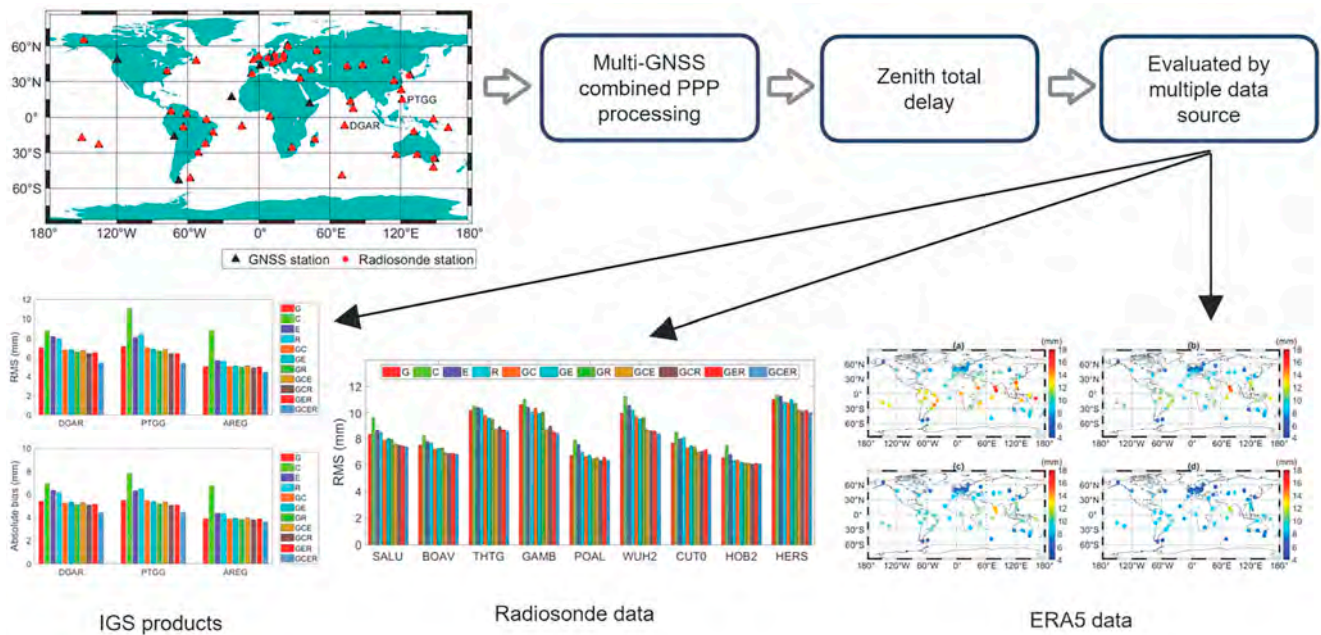
Figure 10. Estimation and evaluation of ZTD from single and multiple GNSS observations (Reprinted from Ref. [24]).
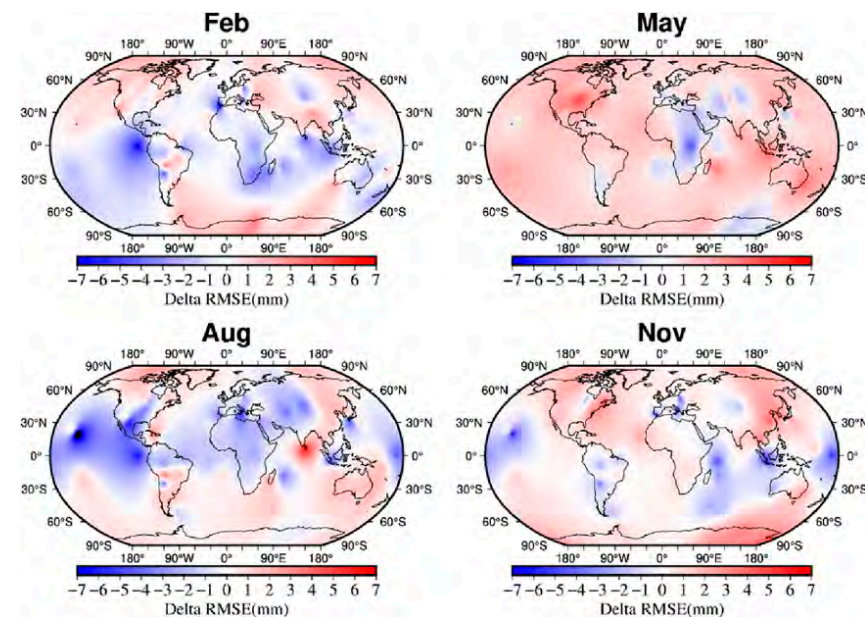

Figure 11. The differences in ZTD RMSE between La Nina and non-La Nina IGS stations (Reprinted with permission from Ref. [48]. 2024 Ye, S.).

3.5. Environmental Remote Sensing by GNSS-R

Environmental remote sensing by space-borne GNSS-R was conducted and assessed, specifically, data from CYGNSS (Cyclone GNSS from NASA). This was accomplished by assessing models that utilize nearly simultaneous observations from a pair of CYGNSS satellites using a double-difference method. For a more comprehensive examination of the findings from this intriguing study, the reader is encouraged to explore the results further [49]. In recent years, GNSS-R has emerged as a robust tool for remote sensing, proving indispensable in numerous applications. This technology utilizes signals that are reflected off the Earth's surface and analyzes them to accurately measure a variety of critical parameters; another relevant study focused on evaluating the retrieval of snow depth in permafrost regions. These areas experience significant changes in ground surface elevation,

as they are subjected to annual cycles of subsidence and uplift caused by the thawing and freezing processes that occur in the active layer of the soil.

3.5.1. Water Level Monitoring

Currently, the use of ground-based GNSS-R for monitoring water levels has been extensively validated. Floods seriously affect human production and life, often causing major economic losses. In cases of extreme weather, the river water level can rise sharply in a short time, which seriously threatens the houses and farmland on both sides of the river. The problem of how to monitor the water level change in real time and timely obtain the water level information for the river is very important. GNSS-R technology instruments have been developed to a high degree in water level monitoring because of their high resolution and the possibility of convenient deployment. Ye et al. [50] employed a weighted iterative least-squares method to estimate high-frequency water level change with multiple systems based on GNSS-R data. By utilizing measured GNSS observation data, a high-frequency water level with impressive centimeter-level accuracy was estimated using multi-frequency and multi-system GNSS-R based on the Signal-to-Noise Ratio (SNR) method. Moreover, the temporal resolution of their findings was remarkably high, with measurements captured at intervals of just five minutes (Figure 12).
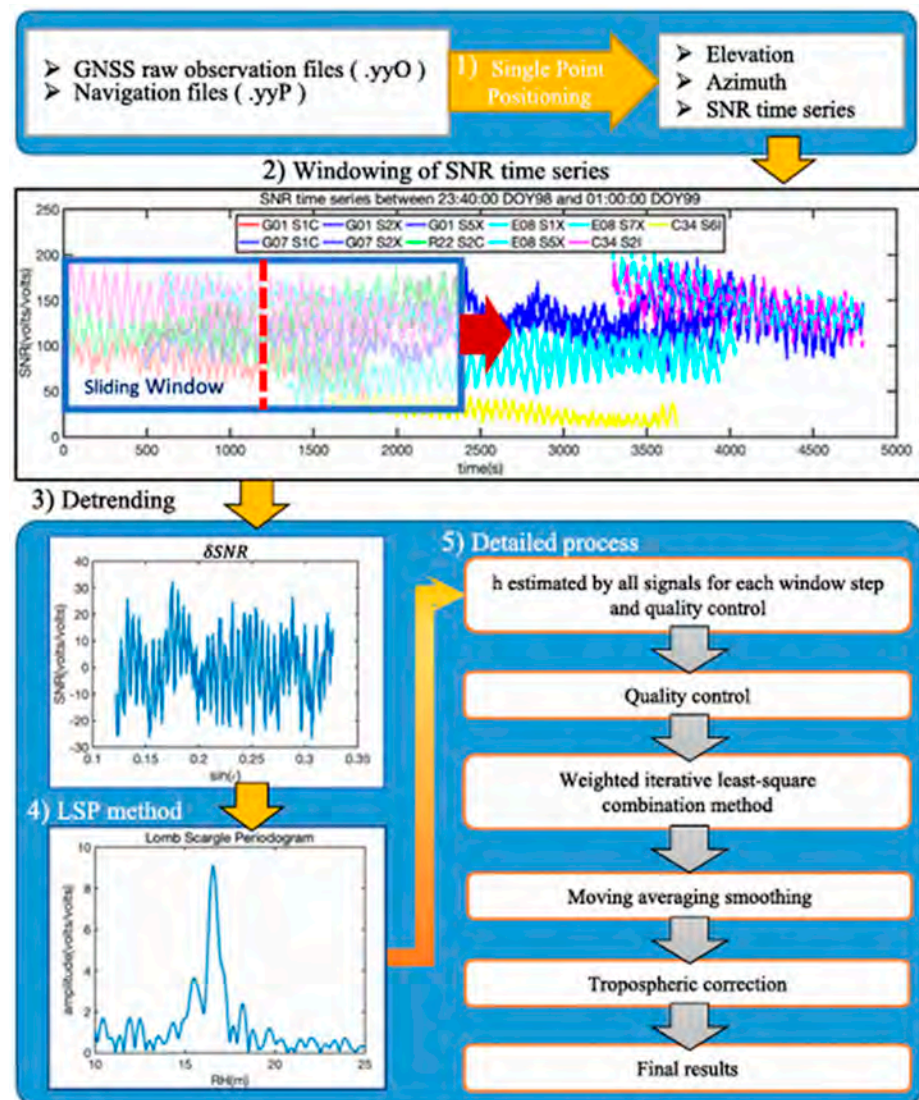

Figure 12. Data processing flow chart for high-frequency GNSS-R water level monitoring (Reprinted with permission from Ref. [50]. 2022 Jin, S.).

Purnell et al. [51] found that GNSS-IR was not as accurate as post-processing in real-time accuracy, but RMSE was significantly improved under a 1 h post-processing delay. In addition, by using a simple tropospheric correction model, the average deviation between GNSS-IR observations and measured data was effectively eliminated. Chen et al. [52] proposed the use of a lower-cost GNSS-IR sensor, that is, to replace the commonly used high-precision GNSS receiver with an electronic device—the mobile phone that we often use. Although the final accuracy was slightly lower than for the control device (CHCNAV P5 GNSS receiver BT560 antenna), the experiment verified the feasibility of the Android smartphone as a GNSS-R sensor.

3.5.2. Typhoon Monitoring

Both wind direction and wind speed are key factors affecting the ocean. The scatterometer functions by emitting electromagnetic wave signals towards the ocean surface and subsequently receiving the reflected signals. This process is critical for retrieving essential data regarding wind speed and direction, which in turn facilitates the detection, estimation, and prediction of typhoons. The effective monitoring of these intense weather systems is heavily reliant on accurately locating the center of a typhoon and predicting its path. These two elements are fundamentally intertwined with the overall quality of forecasts concerning associated thunderstorms and the strong winds that they generate. GNSS-R possesses distinct advantages that make it a valuable tool in atmospheric observation. Notably, it is characterized by both low cost and low power consumption, making it an efficient choice for widespread deployment. When integrated with micro-satellites to create a constellation, GNSS-R can achieve a high spatial and temporal resolution across the globe. This capability enables comprehensive monitoring of weather phenomena. Furthermore, operating within the L-band frequency, GNSS-R is less susceptible to interference from precipitation, rendering it particularly effective for the observation of typhoons. This feature enhances its reliability and accuracy in this context, making it an important asset for meteorological studies.

Ruef [53] created geophysical model functions (GMFs) by utilizing measurement data from CYGNSS, which serves to correlate the observations captured by the CYGNSS GNSS receivers with ocean surface wind speeds. These GMFs are constructed from observational data that closely align with independent assessments of the wind speed at a height of 10 m above the ocean surface. Wang et al. [54] presented a technique for identifying cyclones and estimating their positions utilizing the full delay-Doppler map (FDDM), within which notable changes in asymmetry occur within the cyclone-affected area. Furthermore, by establishing two key features, slope and extremum difference, a detection device for tropical cyclones was introduced. Both the outcomes of simulations and the data from Cyclone GNSS (CYGNSS) demonstrated effective detection capabilities for tropical cyclones monitoring (Figure 13). This research acts as a foundational reference for the leveraging of space-borne GNSS-R technology to directly detect tropical cyclones and to gather real-time data on high wind speeds.

3.5.3. Vegetation Monitoring

The detection of vegetation, including the monitoring of plant water content, is crucial for ensuring healthy crop growth and for the timely identification and resolution of issues. An accurate evaluation of this water content could enhance the precision of soil moisture estimates. With the ongoing advancements in GNSS technology, a dense network of stations has emerged globally, along with an increasing quantity of satellite signals received, aiding in the development of a plant monitoring network. GNSS signals operate within the microwave spectrum and are particularly sensitive to factors such as surface roughness and water content. While these signals assist in monitoring plant water content, they are also influenced by both surface roughness and soil moisture. Consequently, it is essential to utilize techniques that mitigate these interfering variables when estimating plant water content. Larson et al. [55] first proposed the use of the multipath effects of GPS receivers to monitor

soil moisture, which laid the foundation for GPS reflection measurement to monitor plant water content. Wan et al. [56] used airborne GNSS-R to measure soil moisture in farmland, and correctly inverted the spatial variation of soil moisture with the flight trajectory of the machine, but the inversion results were lower than the measured values. Smalle et al. [57] described the relationship between vegetation growth and ground reflection multipath near GPS stations and showed that in two agricultural test sites, vegetation height and water content were negatively correlated with the intensity of ground reflection multipath signals measured by high-precision GPS stations. Chen et al. [58] designed an antenna suitable for GNSS reflection measurements and experiments showed suitable vegetation monitoring in most agricultural environments.
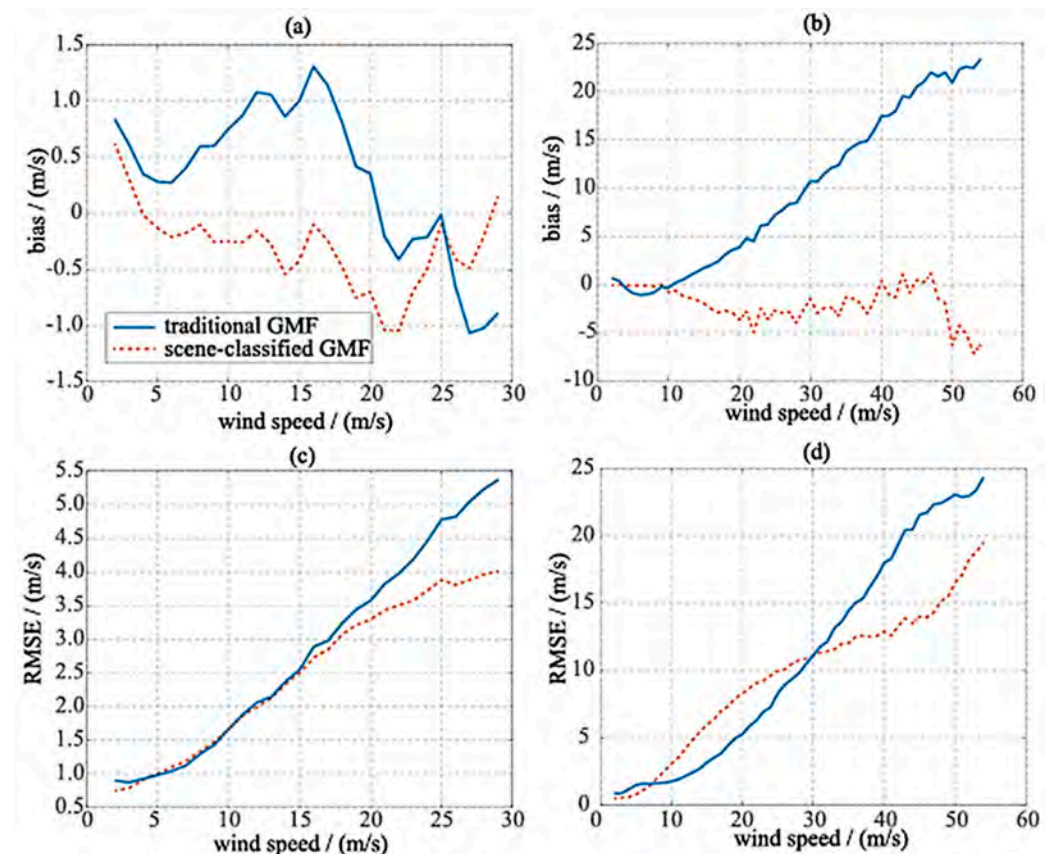

Figure 13. Biases (**a**,**b**) and RMSEs (**c**,**d**) of the retrieved wind speed for (**a**,**c**) cyclone-free and (**b**,**d**) cyclonic conditions (Reprinted with permission from Ref. [54]. 2023 Zhang, G.).

4. Conclusions and Prospects

In this paper, multi-GNSS developments for Earth observation and related applications have been presented, including GNSS navigation and positioning, GNSS RO from FY-3, CYGNSS, FS7/COSMIC-2, PlanetiQ, KOMPSAT-5, PAZ, ZTD for meteorology, ionosphere monitoring, GNSS-R, and various applications. One of the most important results of these studies concerns the definite strengthening of the GNSS technique involved in the field of environmental remote sensing when compared to traditional positioning applications. Over the next few years, future applications will certainly adopt these strategies. Furthermore, Artificial Intelligence (AI) will be further applied in Earth observations and applications associated with GNSS positioning, navigation, timing and remote sensing, in addition to data processing with the use of Machine Learning for the purposes of ground-based and space-borne Earth observation as well as other uses involving Autonomous Navigation Systems.

Also, the development of GNSS-based products, in the context of services such as drones beyond line-of-sight (BVLOS), will play an important role: such drones can work

over greater distances than those limiting traditional ones, even in those areas not easily accessible to humans, or in emergency situations arising due to natural events such as floods or earthquakes. Also, another challenge comes from indoor positioning systems (IPS), which can currently achieve accuracy levels matching with GNSS-RTK (which is used only outdoors), as computer technologies involving wireless access, 5G networking, and 3D mapping of the surrounding environment can meet the requirements of predictive positioning when GNSS data are not forthcoming. Among the most recent applications are Advanced Satellite Earth Observing Technologies for Weather and Climate Resilience, Decision Support Systems for Civil Infrastructure with GNSS Technology, Land Deformation and Engineering Structural Health Monitoring Using Geo-Spatial Technologies, Multi-GNSS PPP, and GNSS for Urban Transport Applications, which will also contribute to increasing the use and potential of GNSS systems.

The progress towards multi-GNSS methods and techniques for Earth observation as well as its emerging applications, are reviewed and presented in details. GNSS technology is not only designed for conventional positioning purposes, and it could also be used more widely in the context of remote sensing. Furthermore, GNSS technology is developing towards high precision, global coverage, multi-frequency and multi-system compatibility. For example, dual-frequency and triple-frequency GNSS receivers have improved anti-interference ability and positioning accuracy, and centimeter-level positioning accuracy is becoming more and more popular. The integration of low-orbit satellites and GNSS, and the deep integration of 5G communication and intelligent driving will also promote the use of GNSS in new application fields, particularly low-altitude economy. With the continuous development of automobile and UAV industry, assisted driving and automatic driving technology have been developed rapidly, and GNSS technology has been extensively deployed in this field. The combined positioning technology of GNSS and INS allows to exploit the advantages of both, enhancing positioning accuracy, stability and reliability, especially in environments where GNSS signals are interfered with or cannot be received. GNSS/INS fusion provides high-precision and continuous positioning for vehicles and drones. Especially in urban environments, INS can maintain stable navigation performance in cases in which GPS signals are blocked by buildings. The development of new sensors, such as quantum INS, to achieve higher accuracy and greater stability of navigation will be a significant upcoming research topic. The advantage of GNSS/INS fusion can reach continuous and high-precision positioning in dynamic, complex, and signal-constrained environments. In the future, with the advancement of technology, these applications will be more extensive [59].

GNSS radio occultation technology also shows great potential in atmospheric and ionospheric monitoring, especially in meteorology and space weather monitoring. It is well known that various GNSS signals are influenced by the Earth's atmosphere, which includes both the troposphere and ionosphere, and these effects have been represented through intricate mathematical models [60]. While atmospheric delays significantly impair the precision of GNSS positioning, a wealth of useful data can be extracted from the GNSS signals that traverse the atmosphere, and can then be utilized in areas such as natural disaster monitoring, weather forecasting, and other domains. GNSS technology is playing an increasingly important role in monitoring extreme weather events, such as typhoons and sea ice monitoring [61]. In typhoon monitoring, GNSS-Reflectometry provides information valuable for disaster warnings, with its significant advantages in obtaining information about typhoons. Errors occur in GNSS signals as they travel through the atmosphere, and these inaccuracies are significantly linked to the level of atmospheric humidity. Through the examination of this delay, researchers are able to gauge the volume of water vapor present in the atmosphere, allowing for predictions regarding the intensity and rainfall associated with typhoons. Additionally, the monitoring of rainstorms gains from the advancements of GNSS technology. GNSS offers crucial data on atmospheric humidity, which is vital for evaluating the intensity and precipitation of rainstorms. By integrating GNSS observational data with precipitation radar information, a more precise estimation

of precipitation intensity and the rainstorm can be accomplished, thereby enhancing the reliability of early warning systems. In monitoring extreme weather phenomena, such as cold waves and droughts, GNSS technology provides valuable data by monitoring changes in humidity and changes in atmospheric structure. These data help scientists to better understand the formation and development of extreme weather phenomena. In general, the application of GNSS technology in extreme weather monitoring has improved the accuracy of weather forecasting and the timeliness of disaster warnings, which are of major relevance for dealing with climate change and protecting public safety. An ionospheric model has been created utilizing GNSS occultation data, and information regarding the electron density profile is acquired by detecting the delay effect evident in satellite signals traversing the ionosphere. These data can be used to construct accurate ionospheric models to help analyze ionospheric variations and improve the accuracy of navigation, communication, and space weather warnings [62,63]. Hence, it is crucial to thoroughly explore the impact of the atmosphere on multi-GNSS positioning applications on the ground and in space (such as BDS, Galileo, GLONASS, GPS, IRNSS, and QZSS) and enhance the ZTD and TEC potential values.

Finally, the GNSS has been extensively implemented in many fields, showing excellent performance in global positioning, navigation, timing, and so on. It plays a key role in transportation, agriculture, fishery management, emergency rescue, and natural disaster monitoring. Especially in precision agriculture, unmanned driving, intelligent logistics, and other aspects, the high-precision GNSS positioning and timing functions have been widely used [64–66]. In the future, the application scope of GNSS will be further expanded, covering the frontier fields of the Internet of Things, the smart city and 5G technology, so as to help the global digital landscape and enhance intelligent development.

Author Contributions: Conceptualization, S.J. and G.D.; methodology, S.J. and X.M.; validation, S.J. and X.M.; formal analysis, S.J. and X.M.; writing—original draft preparation, S.J., G.D., X.M. and Y.Z.; writing—review and editing, S.J., G.D. and Y.Z. All authors have read and agreed to the published version of the manuscript.

Data Availability Statement: GNSS observation data and products can be accessed at https://cddis.nasa.gov/Data_and_Derived_Products/GNSS/GNSS_data_and_product_archive.html (accessed on 10 September 2024). GPS/Galileo/BDS clock/bias products from Wuhan University can be accessed at ftp://igs.gnsswhu.cn/pub/whu/phasebias/ (accessed on 10 September 2024).

Conflicts of Interest: The authors declare no conflicts of interest.

References

1. Jin, S.; Wang, Q.; Dardanelli, G. A Review on Multi-GNSS for Earth Observation and Emerging Applications. *Remote Sens.* **2022**, *14*, 3930. [CrossRef]
2. Jin, S.; Dardanelli, G. (Eds.) *BDS/GNSS for Earth Observation*; MDPI Press: Basel, Switzerland, 2023; 322p, ISBN 978-3-0365-8997-8.
3. BDS/GNSS for Earth Observation: Part, II. Available online: https://www.mdpi.com/journal/remotesensing/special_issues/KPKKS2R3UJ (accessed on 4 October 2024).
4. Su, K.; Jin, S. A Novel GNSS Single-Frequency PPP Approach to Estimate the Ionospheric TEC and Satellite Pseudorange Observable-Specific Signal Bias. *IEEE Trans. Geosci. Remote Sens.* **2022**, *60*, 1–12. [CrossRef]
5. Hu, J.; Liu, W.; Zhu, F.; Tao, X.; Zhang, X. V-RTK: A velocity-constrained RTK algorithm to improve position accuracy of low-cost receiver in urban environments. *Adv. Space Res.* **2023**, *72*, 4721–4734. [CrossRef]
6. Jin, S.; Wang, Q.; Shi, Q. Parameters estimation and applications from single- to five-frequency multi-GNSS Precise Point Positioning, ACTA Geod. *Cartograph. Sin.* **2022**, *51*, 1239–1248.

7. Radicioni, F.; Stoppini, A.; Marconi, L.; Tosi, G. Low-cost multi-frequency GNSS receivers: Performance evaluation for positioning and navigation. *Int. Arch. Photogramm. Remote Sens. Spat. Inf. Sci.—ISPRS Arch.* **2023**, *48*, 167–174. [CrossRef]
8. Baybura, T.; Tiryakioğlu, İ.; Uğur, M.A.; Solak, H.İ.; Şafak, Ş. Examining the Accuracy of Network RTK and Long Base RTK Methods with Repetitive Measurements. *J. Sens.* **2019**, *2019*, 3572605. [CrossRef]
9. Lu, Y.; Ji, S.; Tu, R.; Weng, D.; Lu, X.; Chen, W. An Improved Long-Period Precise Time-Relative Positioning Method Based on RTS Data. *Sensors* **2021**, *21*, 53. [CrossRef]
10. Zhang, B.; Odijk, D. A method for processing GNSS data from regional reference networks to enable single-frequency PPP-RTK. *Acta Geophys. Sin.* **2015**, *58*, 2306–2319.
11. Pipitone, C.; Maltese, A.; Lo Brutto, M.; Dardanelli, G. A Review of Selected Applications of GNSS CORS and Related Experiences at the University of Palermo (Italy). *Remote Sens.* **2023**, *15*, 5343. [CrossRef]
12. Angrisano, A.; Dardanelli, G.; Innac, A.; Pisciotta, A.; Pipitone, C.; Gaglione, S. Performance Assessment of PPP Surveys with Open Source Software Using the GNSS GPS–GLONASS–Galileo Constellations. *Appl. Sci.* **2020**, *10*, 5420. [CrossRef]
13. Dardanelli, G.; Maltese, A.; Pipitone, C.; Pisciotta, A.; Lo Brutto, M. NRTK, PPP or Static, That Is the Question. Testing Different Positioning Solutions for GNSS Survey. *Remote Sens.* **2021**, *13*, 1406. [CrossRef]
14. Dardanelli, G.; Pipitone, C. The effects of CORS network geometry and differential NRTK corrections on GNSS solutions. *Geogr. Tech.* **2021**, *16*, 56–69. [CrossRef]
15. Pipitone, C.; Dardanelli, G.; Lo Brutto, M.; Bruno, V.; Mattia, M.; Guglielmino, F.; Rossi, M.; Barreca, G. Use of CORS Time Series for Geodynamics Applications in Western Sicily (Italy). *Commun. Comput. Inf. Sci.* **2020**, *1246*, 61–76.
16. Kouba, J.; Héroux, P. Precise Point Positioning Using IGS Orbit and Clock Products. *GPS Solut.* **2001**, *5*, 12–28. [CrossRef]
17. Zumberge, J.F.; Heflin, M.B.; Jefferson, D.C.; Watkins, M.M.; Webb, F.H. Precise point positioning for the efficient and robust analysis of GPS data from large networks. *J. Geophys. Res. Solid Earth* **1997**, *102*, 5005–5017. [CrossRef]
18. Gao, Y.; Shen, X. Improving ambiguity convergence in carrier phase-based precise point Positioning. In Proceedings of the ION GPS, Salt Lake City, UT, USA, 11–14 September 2001; pp. 1532–1539.
19. Li, H.; Zhu, G.; Huang, L.; Mo, Z.; Kang, Q. An improved method for developing the precipitable water vapor vertical correction global grid model. *Atmos. Res.* **2024**, *311*, 107664. [CrossRef]
20. Wang, Y.; Jin, S. Effect of GNSS radio occultation observations on the prediction of the 2021 Henan rainstorm. *GPS Solut.* **2023**, *27*, 102. [CrossRef]
21. Chen, P.; Yao, W.; Zhu, X. Combination of Ground- and Space-Based Data to Establish a Global Ionospheric Grid Model. *IEEE Trans. Geosci. Remote Sens.* **2015**, *53*, 1073–1081. [CrossRef]
22. Chen, P.; Yao, Y.; Yao, W. Global ionosphere maps based on GNSS, satellite altimetry, radio occultation and DORIS. *GPS Solut.* **2017**, *21*, 639–650. [CrossRef]
23. Su, K.; Jin, S. Improvement of Multi-GNSS Precise Point Positioning Performances with Real Meteorological Data. *J. Navig.* **2018**, *71*, 1–17. [CrossRef]
24. Xia, S.; Jin, S.; Jin, X. Estimation and Evaluation of Zenith Tropospheric Delay from Single and Multiple GNSS Observations. *Remote Sens.* **2023**, *15*, 5457. [CrossRef]
25. Jin, S.G.; Han, L.; Cho, J. Lower atmospheric anomalies following the 2008 Wenchuan Earthquake observed by GPS measurements. *J. Atmos. Sol.-Terr. Phys.* **2011**, *73*, 810–814. [CrossRef]
26. Wu, M.; Jin, S.; Li, Z.; Cao, Y.; Ping, F.; Tang, X. High-Precision GNSS PWV and Its Variation Characteristics in China Based on Individual Station Meteorological Data. *Remote Sens.* **2021**, *13*, 1296. [CrossRef]
27. Lavers, D.A.; Simmons, A.; Vamborg, F.; Rodwell, M.J. An evaluation of ERA5 precipitation for climate monitoring. *Q. J. R. Meteorol. Soc.* **2022**, *148*, 3152–3165. [CrossRef]
28. Zhao, X.; Niu, Q.; Chi, Q.; Chen, J.; Liu, C. A new LSTM-based model to determine the atmospheric weighted mean temperature in GNSS PWV retrieval. *GPS Solut.* **2024**, *28*, 74. [CrossRef]
29. Dabove, P.; Bagheri, M. Enhancing Atmospheric Monitoring Capabilities: A Comparison of Low- and High-Cost GNSS Networks for Tropospheric Estimations. *Remote Sens.* **2024**, *16*, 2223. [CrossRef]
30. Wang, J.; Yu, X.; Aragon-Angel, A.; Rovira-Garcia, A.; Wang, H. The Selection of Basic Functions for a Time-Varying Model of Unmodeled Errors in Medium and Long GNSS Baselines. *Remote Sens.* **2023**, *15*, 5022. [CrossRef]
31. Gučević, J.; Delčev, S.; Vasović Šimšić, O. Practical Limitations of Using the Tilt Compensation Function of the GNSS/IMU Receiver. *Remote Sens.* **2024**, *16*, 1327. [CrossRef]
32. Chen, M.; Zhao, L.; Zhai, W.; Lv, Y.; Jin, S. Assessment of the Real-Time and Rapid Precise Point Positioning Performance Using Geodetic and Low-Cost GNSS Receivers. *Remote Sens.* **2024**, *16*, 1434. [CrossRef]
33. Cui, B.; Wang, J.; Li, P.; Ge, M.; Schuh, H. Modeling wide-area tropospheric delay corrections for fast PPP ambiguity resolution. *GPS Solut.* **2022**, *26*, 56. [CrossRef]
34. Xiao, G.; Yang, C.; Wei, H.; Xiao, Z.; Zhou, P.; Li, P.; Dai, Q.; Zhang, B.; Yu, C. PPP ambiguity resolution based on factor graph optimization. *GPS Solut.* **2024**, *28*, 178. [CrossRef]
35. Li, W.; Sun, Y.; Bai, W.; Du, Q.; Wang, X.; Wang, D.; Liu, C.; Li, F.; Kang, S.; Song, H. A Novel Approach to Evaluate GNSS-RO Signal Receiver Performance in Terms of Ground-Based Atmospheric Occultation Simulation System. *Remote Sens.* **2024**, *16*, 87. [CrossRef]

36. Zhran, M.; Mousa, A.; Wang, Y.; Hasher, F.F.; Jin, S. Assessment of Commercial GNSS Radio Occultation Performance from PlanetiQ Mission. *Remote Sens.* **2024**, *16*, 3339. [CrossRef]

37. Wang, Q.; Zhu, J.; Hu, F. Ionosphere Total Electron Content Modeling and Multi-Type Differential Code Bias Estimation Using Multi-Mode and Multi-Frequency Global Navigation Satellite System Observations. *Remote Sens.* **2023**, *15*, 4607. [CrossRef]

38. Poniatowski, M.; Nykiel, G.; Borries, C.; Szmytkowski, J. Spatio-Temporal Validation of GNSS-Derived Global Ionosphere Maps Using 16 Years of Jason Satellites Observations. *Remote Sens.* **2023**, *15*, 5053. [CrossRef]

39. Zhang, Q.; Zhao, Q. Global Ionosphere Mapping and Differential Code Bias Estimation during Low and High Solar Activity Periods with GIMAS Software. *Remote Sens.* **2018**, *10*, 705. [CrossRef]

40. Tsai, L.-C.; Su, S.-Y.; Schuh, H.; Alizadeh, M.M.; Wickert, J. Seasonal–Longitudinal Variability of Equatorial Plasma Bubbles Observed by FormoSat-7/Constellation Observing System for Meteorology Ionosphere and Climate II and Relevant to the Rayleigh–Taylor Instability. *Remote Sens.* **2024**, *16*, 2310. [CrossRef]

41. Aa, E.; Zou, S.; Liu, S. Statistical analysis of equatorial plasma irregularities retrieved from Swarm 2013–2019 observations. *J. Geophys. Res. Space Phys.* **2020**, *125*, e2019JA027022. [CrossRef]

42. Zhao, X.; Li, G.; Hu, L.; Xie, H.; Sun, W.; Li, Y.; Ning, B.; Liu, L. Solar and geomagnetic activity and seasonal dependence of global equatorial plasma bubbles based on GNSS observations. *Chin. J. Geophys.* **2023**, *66*, 2703–2712. (In Chinese) [CrossRef]

43. Li, W.; Wang, K.; Yuan, K. Performance and Consistency of Final Global Ionospheric Maps from Different IGS Analysis Centers. *Remote Sens.* **2023**, *15*, 1010. [CrossRef]

44. Jiang, H.; Jin, S.; Huo, X.; Xi, H.; An, J.; Liu, J.; Sang, W.; Guo, Q. A Dual-Layer Ionosphere Model Based on 3-D Ionospheric Constraint. *IEEE Trans. Geosci. Remote Sens.* **2024**, *62*, 1–13. [CrossRef]

45. Li, L.; Jin, S.; Yuan, L. A Multi-Parameter Global Electron Density Model (GEDM) from GNSS Radio Occultation Data. *IEEE Trans. Geosci. Remote Sens.* **2024**, *62*, 1–10. [CrossRef]

46. Han, Y.; Wang, L.; Chen, R.; Fu, W.; Li, T.; Zhou, H. Toward real-time construction of global ionosphere map from ground and space-borne observations. *GPS Solut.* **2022**, *26*, 147. [CrossRef]

47. Ma, M.; Jin, S.; Jin, X.T. Characteristics of ionospheric disturbances during the 2021 Typhoon Chanthu based on GPS and GLONASS. *Adv. Space Res.* **2024**, *74*, 271–283. [CrossRef]

48. Fan, Y.; Xia, F.; Ye, S.; Hu, F.; Luo, H.; Sha, Z. Analysis of GNSS-ZTD retrieval using dual-frequency raw observations. *Measurement* **2024**, *231*, 114597. [CrossRef]

49. Powell, C.E.; Ruf, C.S.; McKague, D.S.; Wang, T.; Russel, A. An Instrument Error Correlation Model for Global Navigation Satellite System Reflectometry. *Remote Sens.* **2024**, *16*, 742. [CrossRef]

50. Ye, M.; Jin, S.; Jia, Y. Ten-Minute Sea-Level Variations from Combined Multi-GNSS Multipath Reflectometry Based on a Weighted Iterative Least-Square Method. *IEEE Trans. Geosci. Remote Sens.* **2022**, *60*, 1–10. [CrossRef]

51. Purnell, D.; Gomez, N.; Minarik, W.; Langston, G. Real-Time Water Levels Using GNSS-IR: A Potential Tool for Flood Monitoring. *Geophys. Res. Lett.* **2024**, *51*, e2023GL105039. [CrossRef]

52. Chen, L.; Chai, H.; Zheng, N.; Wang, M.; Xiang, M. Feasibility and performance evaluation of low-cost GNSS devices for sea level measurement based on GNSS-IR. *Adv. Space Res.* **2023**, *72*, 4651–4662. [CrossRef]

53. Ruf, C.S.; Balasubramaniam, R. Development of the CYGNSS Geophysical Model Function for Wind Speed. *IEEE J. Sel. Top. Appl. Earth Obs. Remote Sens.* **2019**, *12*, 66–77. [CrossRef]

54. Wang, F.; Zhang, G.; Yang, D.; Kuang, H. Single-Pass Tropical Cyclone Detector and Scene-Classified Wind Speed Retrieval Model for Spaceborne GNSS Reflectometry. *IEEE Trans. Geosci. Remote Sens.* **2023**, *61*, 1–16. [CrossRef]

55. Larson, K.M.; Small, E.E.; Gutmann, E.; Bilich, A.; Axelrad, P.; Braun, J. Using GPS multipath to measure soil moisture fluctuations: Initial results. *GPS Solut.* **2008**, *12*, 173–177. [CrossRef]

56. Wan, W.; Bai, W.; Zhao, L.; Long, D.; Sun, Y.; Meng, X.; Chen, H.; Cui, X.; Hong, Y. Initial results of China's GNSS-R airborne campaign: Soil moisture retrievals. *Sci. Bull.* **2015**, *60*, 964–971. [CrossRef]

57. Small, E.E.; Larson, K.M.; Braun, J.J. Sensing vegetation growth with reflected GPS signals. *Geophys. Res. Lett.* **2010**, *37*. [CrossRef]

58. Chen, Q.; Won, D.; Akos, D.M.; Small, E.E. Vegetation Sensing Using GPS Interferometric Reflectometry: Experimental Results With a Horizontally Polarized Antenna. *IEEE J. Sel. Top. Appl. Earth Obs. Remote Sens.* **2016**, *9*, 4771–4780. [CrossRef]

59. Zhang, G.; Hsu, L.-T. Intelligent GNSS/INS integrated navigation system for a commercial UAV flight control system. *Aerosp. Sci. Technol.* **2018**, *80*, 368–380. [CrossRef]

60. Zhang, J.; Zuo, X.; Guo, S.; Xie, S.; Yang, X.; Li, Y.; Yue, X. A New Grid Zenith Tropospheric Delay Model Considering Time-Varying Vertical Adjustment and Diurnal Variation over China. *Remote Sens.* **2024**, *16*, 2023. [CrossRef]

61. Jin, S.; Camps, A.; Jia, Y.; Wang, F.; Martin-Neira, M.; Huang, F.; Yan, Q.; Zhang, S.; Li, Z.; Edokossi, K.; et al. Remote sensing and its applications using GNSS reflected signals: Advances and prospects. *Satell. Navig.* **2024**, *5*, 19. [CrossRef]

62. Swarnalingam, N.; Wu, D.L.; Emmons, D.J.; Gardiner-Garden, R. Optimal Estimation Inversion of Ionospheric Electron Density from GNSS-POD Limb Measurements: Part II-Validation and Comparison Using NmF2 and hmF2. *Remote Sens.* **2023**, *15*, 4048. [CrossRef]

63. Hoque, M.M.; Prol, F.S.; Hernandez-Pajares, M.; Notarpietro, R.; Yuan, L.; Olivares-Pulido, G.; Graffigna, V.; Von Engeln, A.; Marquardt, C. Assessment of GRAS Ionospheric Measurements for Ionospheric Model Assimilation. *Remote Sens.* **2023**, *15*, 3129. [CrossRef]

64. Geng, T.; Li, Z.; Xie, X.; Liu, W.; Li, Y.; Zhao, Q. Real-time ocean precise point positioning with BDS-3 service signal PPP-B2b. *Measurement* **2022**, *203*, 111911. [CrossRef]

65. Jin, S. Preface: BeiDou Navigation Satellite System (BDS)/GNSS+: New developments and emerging applications. *Adv. Space Res.* **2017**, *60*, 2519. [CrossRef]

66. Xiao, P.; Sun, F.; Wang, K.; Xiao, K.; Shang, X.; Liu, J. Positioning performance analysis of real-time BDS-3 PPP-B2b/INS tightly coupled integration in urban environments. *Adv. Space Res.* **2023**, *72*, 4008–4020. [CrossRef]